submitted to *Remote Sensing*

A new index for the volcanic explosion scales using impulsive ionospheric disturbances

[1]Mokhamad Nur Cahyadi, [1]Eko Yuli Handoko,[1]Ririn Wuri Rahayu, & [2]Kosuke Heki

[1] Dept. Geomatic Engineering, ITS, Surabaya, Indonesia
[2] Dept. Earth Planet. Sci., Hokkaido University, Sapporo, Japan

Abstract: Using the total ionospheric electron content (TEC) data from ground-based global satellite navigation system (GNSS) receivers in Japan, we compared ionospheric responses to five explosive volcanic eruptions 2004-2015 of the Asama, Shin-Moe, Sakura-jima, and Kuchinoerabu-jima volcanoes. The TEC records show N-shaped disturbances with a period ~80 seconds propagating outward with the acoustic wave speed of ~0.8 km/s from the volcanoes. The amplitudes of these TEC disturbances are a few percent of the background absolute TEC, and we propose to use such relative amplitudes as a new index for the intensity of volcanic explosions.

Keywords: Ionospheric disturbance; Asama; Shin-Moe; Sakurajima; Kuchinoerabujima; volcanic explosion, index

---

1. Introduction

The Earth's ionosphere ranges from 60 to 1,000 km in altitude and is characterized by large number of free electrons. Ionospheric conditions are controlled by solar radiation and often disturbed by geomagnetic activities. In addition to such disturbances caused by space weather, the ionosphere is disturbed by events below (Blanc, 1985), such as earthquakes (Heki, 2020), tsunami (Occhipinti et al., 2013), and volcanic eruptions.

Ionospheric total electron content (TEC) can be easily measured by comparing the phases of two microwave carriers from global navigation satellite system (GNSS) satellites, such as Global Positioning System (GPS) (e.g. Hofmann-Wellenhof et al., 2008). Ground GNSS networks have been deployed to monitor crustal movements, and these networks were found useful to study ionospheric disturbances by volcanic eruptions. There are two types of ionospheric TEC responses to various types of volcanic eruptions.

The first type is the long-lasting harmonic TEC oscillations (Figure 1). It was found after the 13 July 2003 eruption of the Soufrière Hills volcano, Montserrat, in the Lesser Antilles (Dautermann et al., 2003a, b), and after the February 2014 eruption of the Kelud volcano, eastern Java Island, Indonesia (Nakashima et al., 2016). They reported that harmonic oscillations caused by atmospheric resonance excited by the Plinian eruption of the Kelud volcano lasted for ~ 2.5 hours after the eruption started. Shults et al. (2016) found similar TEC oscillations after the 2015 April Plinian eruption of the Calbuco volcano, Chile. Cahyadi et al. (2020) also found such harmonic TEC oscillations lasting ~20 minutes following the

2010 November 5 eruption of the Merapi volcano, central Java Island. They suggested that the TEC oscillation amplitudes relative to background TEC represent the mass eruption rate, and the products of such amplitudes and the duration provides an index for the total amount of the ejecta.

The second type of disturbances occur 8-10 minutes after volcanic explosions by acoustic waves propagating upward from the surface to ionospheric F region (Figure 1). They make short-term N-shaped impulsive TEC responses as Heki (2006) observed with the GPS-TEC method after the Vulcanian explosive eruption of the Asama volcano, Central Japan, on September 1, 2004. In this work, we focus on the impulsive ionospheric responses to this type of volcanic explosions.

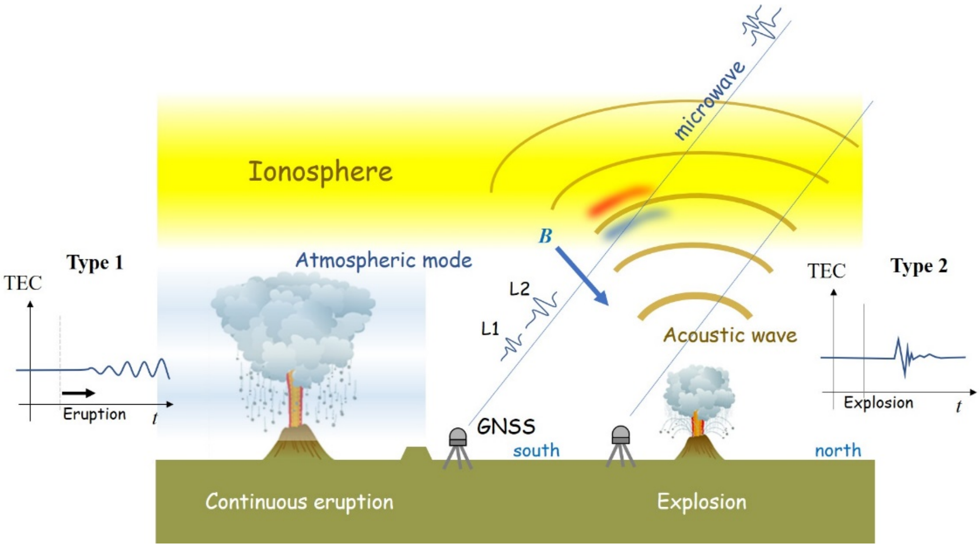

Figure 1. Ionospheric disturbance caused by continuous (Type 1 left) and explosive (Type 2 right) volcanic eruptions can be detected by differential ionospheric delays of microwave signals of two carrier frequencies (L1 and L2) from GNSS satellites. Strong continuous eruptions sometimes excite atmospheric modes and long-term oscillatory disturbances in ionosphere. For explosive eruptions, we often find short-term impulsive disturbances in ionosphere 8-10 minutes after eruptions, the time required for acoustic waves to reach the ionospheric F region. The acoustic wave makes electron density anomalies (pairs of positive and negative anomalies as shown with red and blue colors in the figure) on the southern side of the volcano (for northern hemisphere cases).

Intensity of a volcanic explosion has been studied by atmospheric pressure changes associated with the airwave (infrasound) generated by the eruption (e.g. Matoza et al., 2019). However, geometric settings of such sensors relative to volcanoes are diverse, and amplitudes of such airwaves are difficult to serve as a universal index to describe the explosion intensity. In this study, we explore the possibility to use the amplitude of ionospheric disturbance that occur ~10 minutes after a large explosion as the new index. For this purpose, we compare ionospheric TEC responses to five recent explosive volcanic eruptions of four volcanoes in Japan 2004-2015 comparing the GNSS-TEC data from GEONET (GNSS Earth Observation Network), a dense GNSS network in Japan.

2. GNSS data

We calculated TEC by multiplying a certain factor to the phase difference of the microwave signals in two frequencies, L1 (~1.5 GHz) and L2 (~1.2 GHz), from GNSS receivers in the Japanese GEONET. TEC indicates number of electrons integrated along the line-of-sight (LoS) connecting the ground stations and GNSS satellites. We often represent the point of observation using the latitude and longitude of ionospheric piercing point (IPP), the point of intersection of LoS with the hypothetical thin layer assumed at the altitude of the highest electron density (~300 km). We plot their surface projections, often called sub-ionospheric points (SIP), on the map. In this study, we used only GPS satellites. The details of the GNSS-TEC technique to study lithospheric phenomena are available in the review article by Heki (2020).

We downloaded the raw GNSS data on the days of the eruptions from terras.gsi.go.jp. To remove the integer ambiguity of phase observables, the TEC obtained from carrier phases are adjusted to those from pseudo-ranges without such ambiguities. Such slant TEC (STEC) values are often converted to vertical TEC (VTEC) after removing inter-frequency biases in GNSS receivers and satellites. Here, however, we use STEC throughout the study in order to capture TEC signatures from LoS penetrating the wavefront with shallow angles (Figure 1).

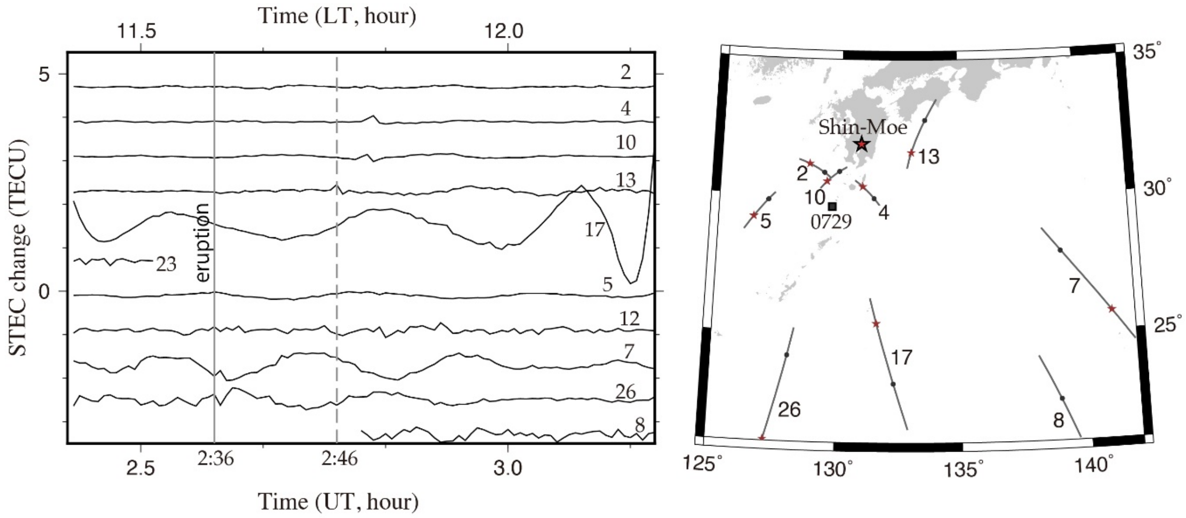

Figure 2. STEC changes observed at the GNSS station 0729 (square in the map) over 2.4-3.2 UT, February 11, 2011. An explosive eruption of the Shin-Moe volcano (star in the map) occurred at 2:36 UT (solid vertical line), and small ionospheric observations are seen to occur in signals with GPS satellites 4, 10, and 13 around 10 minutes after the eruption (dashed vertical line). In the map, we show the trajectory of SIPs with solid circles and red stars indicating the 3:00 UT and 2:36 UT, respectively.

Interaction of the electron movement with geomagnetic fields allows us to observe such TEC disturbances from stations located to the south of volcanoes (e.g. see Rolland et al., 2013). Figure 2 shows an example of the STEC change time series before and after the 2011 February 11 eruption of the Shin-Moe volcano in Kyushu, SW Japan, observed at the station 0729 located in a small island to the south of Kyushu. We isolated the short-term signals by fitting the polynomials (with degree 7) to STEC time series and showing residuals from such reference curves. Small pulses occurring ~10 minutes after the eruption (Satellites 4, 10, 13) are caused by acoustic waves propagating from the volcano to the ionosphere. Incessant small fluctuations of TEC observed by Satellites 7, 8, 12, 17, and 26 are natural variabilities of TEC intrinsic for low elevation satellites.

3. Five volcanic explosions of four volcanoes in Japan

We selected five recent explosive volcanic eruptions in Japan with clear TEC disturbance signals. The Asama volcano, central Japan, started eruptive activity at 11:02 UT on September 1, 2004, with a Vulcanian explosion associated with strong airwaves (Nakada et al., 2005). For this eruption, there have been reports of ionospheric disturbance using GNSS-TEC by Heki (2006) and by HF-Doppler measurements by Chonan et al. (2018). Plume height was unknown due to cloudy weather, and they detected the atmospheric pressure change exceeding 205 Pa at a sensor located 8 km to the south (Yokoo et al., 2005).

Sakura-jima is an active stratovolcano in the Kagoshima Prefecture, Kyushu, and is one of the most active volcanoes in SW Japan. Since 2009, several hundreds of explosions occur every year in the volcano. There were 125 eruptions in 2009 October, in which 101 were explosive. The explosion of Minamidake, Sakurajima, at 07:45 UT on October 3, 2009, was one of the strongest eruptions in its activity since 2009. Plume reached the height ~3,000 m above the caldera rim, and the atmospheric pressure change exceeding 294.5 Pa was detected at a sensor 5 km southeastward. At another observatory, 11 km to the west of the vent, pressure change of 74 Pa was observed (JMA, 2010).

Shin-Moe Volcano is also located in the Kagoshima Prefecture, Kyushu. We studied two explosive eruptions in 2011. In the first eruption (Jan. 31 22:54 UT), the plume reached the height of 2,000 m above the caldera rim, and the atmospheric pressure change exceeding 458.5 Pa was observed at a sensor 2.6 km southwestward. In the second eruption (Feb. 11, 02:36 UT), the plume reached the height of 2,500 m above the caldera rim, and the atmospheric pressure change exceeding 244.3 Pa was observed at the same sensor (JMA, 2013).

The last volcanic eruption was Kuchinoerabu-jima volcano, located at a tiny island Kuchinoerabu-jima ~100 km to the south of Kyushu. The eruption occurred on 3 January 2015 (00:59 UT). The plume height was 9,000 m, and pyroclastic flow reached the ocean. An atmospheric pressure of 62.2 Pa was observed at a sensor located 2.3 km northeastward (JMA, 2015). Nakashima (2018) studied ionospheric disturbances caused by this eruption by using 1 Hz high-rate GNSS data.

4. Comparison of ionospheric disturbances by the five volcanic explosions

Figure 3 compares the impulsive TEC changes with periods of 1-2 minutes, ~10 minutes after the explosion. They are all STEC and the time series show the residual from the best-fit polynomials with degrees 7-9. We also see faint harmonic oscillations (similar to Type 1 disturbance in Figure 1) sometimes follow the eruptions, e.g. the 2015 Kuchinoerabu-jima eruption. Here, we focus on the N-shaped TEC disturbances.

Strong disturbances can be seen only from GNSS stations located to the south of the stations due to the interaction with geomagnetic fields. Therefore, we could not fully take advantage of the dense GNSS network because the Sakura-jima, Shin-Moe and Kuchinoerabu-jima volcanoes are all located in southern Kyushu and GNSS stations are sparse to their south.

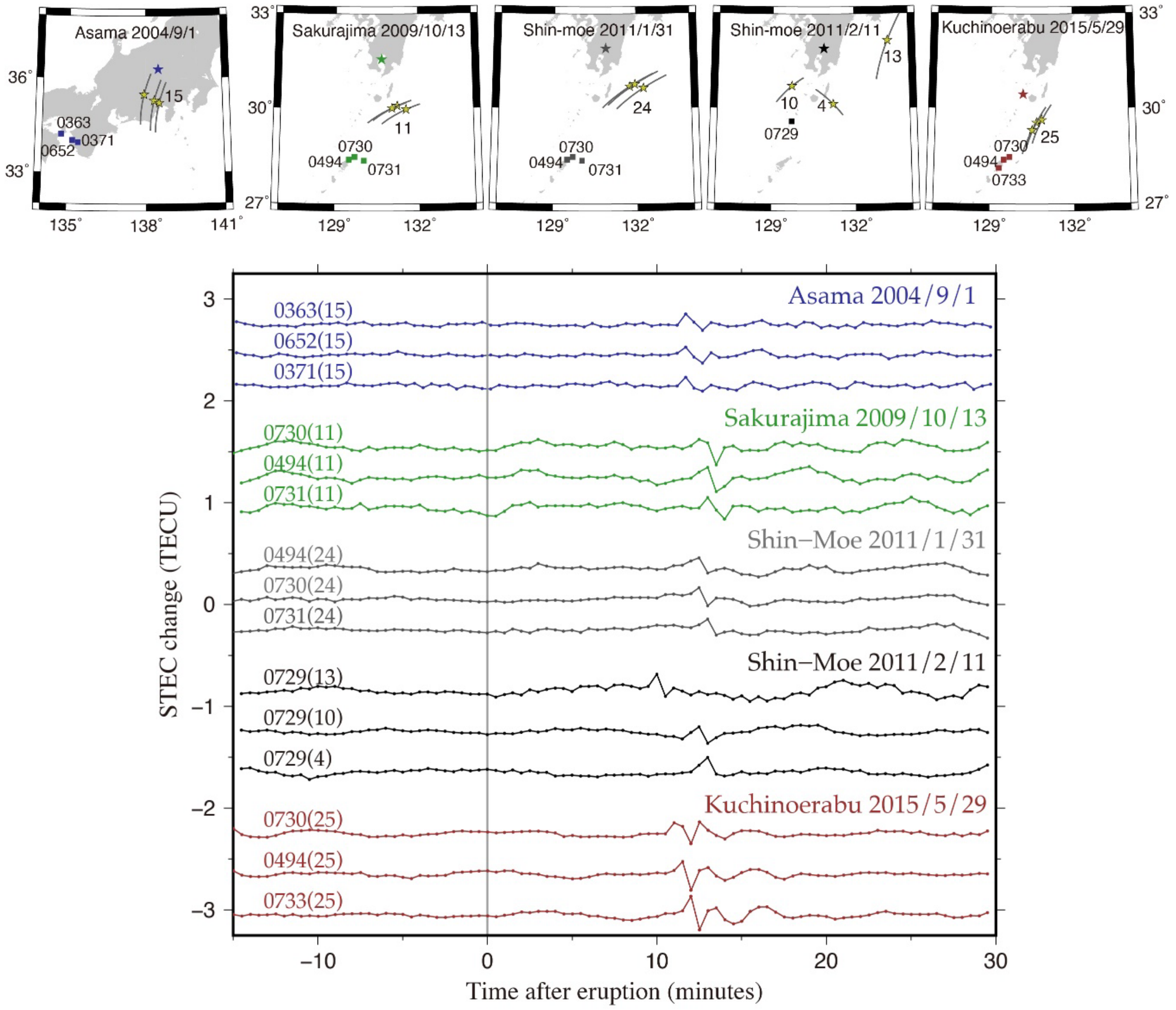

Figure 3. (top) Geometry of volcanoes (large stars), SIP tracks (gray curves) and SIP positions at the time of the eruptions (smal yellow stars), and GNSS stations (squares). We show the STEC time series for the three pairs of stations and satellites (three satellites from one station for the second Shin-Moe eruption, and one satellite from three stations for the rest) for each of the five examples of explosive eruptions in Japan. (bottom) High-pass filtered STEC changes over 45 minutes periods (from 15 minutes before eruption to 30 minutes after eruption) for the five explosive eruptions studied here. Small disturbances can be seen 10-15 minutes after the eruptions.

Following Heki (2006), we try to adjust a simple function

$$f(t) = -at\exp\left(\frac{-t^2}{2\sigma^2}\right), \tag{1}$$

made of a set of positive and negative pulses (a curve in red in the middle of Figure 4), to the disturbances observed by five eruptions in Figure 3. This function has a maximum and minimum at $t=-\sigma$ and $t=\sigma$, respectively. The two parameters a and σ, representing the amplitude and period, respectively, were tuned to minimize the root-mean-squares (rms) of differences between the synthesized and the observed disturbances. The values $\sigma=19.5$ resulted in good fits to the majority of time series, which corresponds to 78 seconds (1.3 minutes) as the approximate period (i.e. $4 \times \sigma$) of the disturbance. From the adjusted values of a , we obtained the peak-to-peak amplitude, i.e. $f(-\sigma)-f(\sigma)$, as summarized in Figure 5. Here we do not discuss the propagation velocity of the ionospheric disturbances because they are known to propagate in the acoustic wave velocity (~0.8 km/s) in the ionospheric F region (Heki, 2006). The same calculation has been done for all the three examples from each eruption and the average peak-to-peak amplitudes are compared in Figure 5.

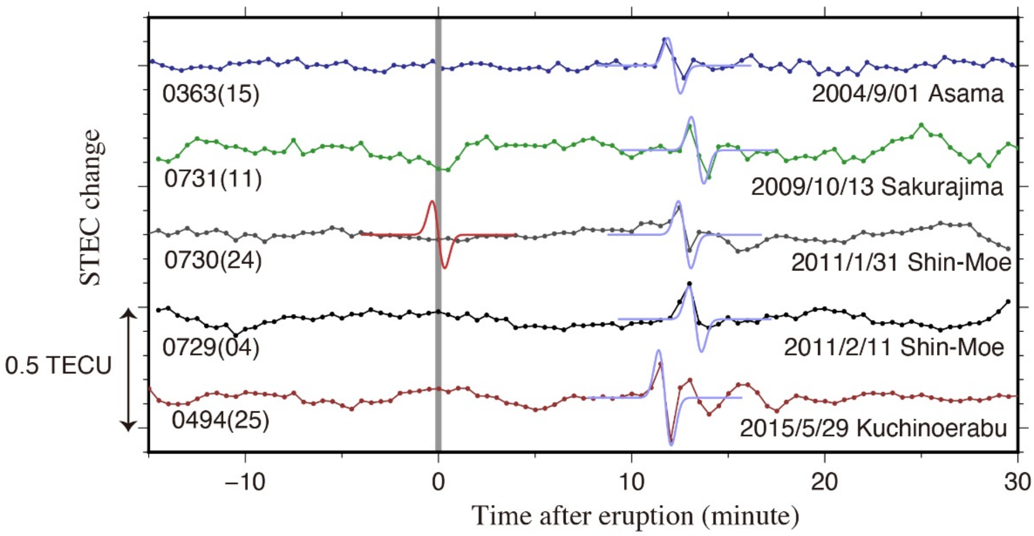

Figure 4. Fit of the model function (shown as a red curve in the middle) to one of the STEC curves in Figure 3 for each eruption. The period of the TEC fluctuation (Heki, 2006) is fixed to 1.3 minutes, and adjusted the amplitudes and time lags to minimize the difference between the model function and the observed TEC.

Volcanic eruptions excite acoustic waves in neutral atmosphere layer and ionospheric electrons move together with such neutral atmospheric molecules. Naturally, the strength of the TEC disturbances is largely influenced by the electron density in the F region of the ionosphere. In order to study objective index for the explosion intensity, it will be reasonable to normalize the amplitudes of STEC changes with background electron densities in the F region. Here we used background VTEC to normalize such amplitudes and express the TEC amplitudes relative to them (blue squares in Figure 5). VTEC values at the time and location of eruptions are obtained from Global Ionospheric Maps (GIM; Mannucci et al. 1998).

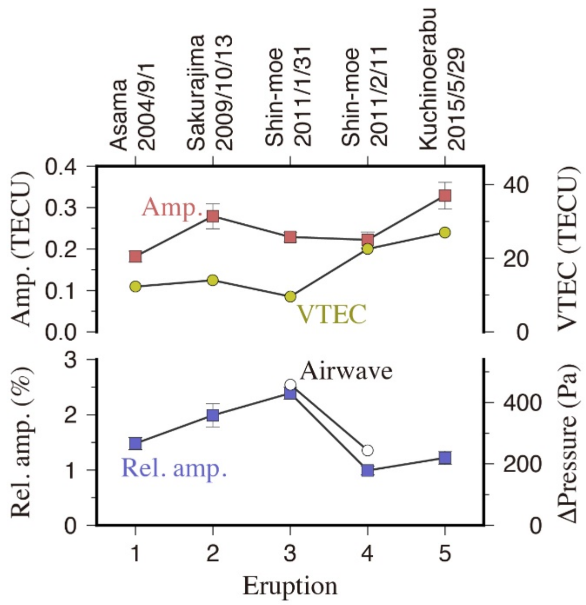

Figure 5. Comparison of the TECs (shown in Figure 3) in absolute (red) and relative (i.e. ration to the background VTEC) (blue) amplitudes. The yellow circles show VTEC values at the time and place of the eruptions calculated using global ionospheric models. For the two eruptions of the Shin-Moe volcano, we compare amplitudes in atmospheric pressure changes detected by the same sensor ~2.6 km from the volcano caused by airwaves by the explosions.

5. Discussion

Intensities of the explosive volcanic eruptions can be studied by measuring amplitudes of airwaves excited by the explosions as atmospheric pressure changes. However, different distance of the ground sensors from the volcanoes and different topographic conditions make it difficult to compare such intensities for different volcanoes. In Figure 5, we compare atmospheric pressure changes by the airwaves for the the January 31 and February 11 explosions of the Shin-Moe volcano detected using the same sensor at the YNN station (JMA, 2011).

As seen in Figure 5, these two eruptions show similar amplitudes of STEC changes. However, the background VTEC at the time of the February eruption was more than twice as strong as those in the January eruption. Hence, relative amptlitude of the January eruption becomes twice as large as the February eruption. This is in agreement with the difference of the pressure changes for these two eruptions (458.5 Pa for the January 31 eruption, and 244.3 Pa for the February 11 eruption).

This suggests the validity of using the relative amplitudes of the ionospheric STEC changes as the new index to describe the intensities of volcanic explosions for different volcanoes. Its benefit is that we do not rely on the deployment of infrasound sensors, i.e. we can use this index whenever enough number of continuous GNSS stations are available on the southern/northern side of the volcano in northern/southern hemisphere. Its drawback is that this index can be used only for strong volcanic explosions occurring when number of ionospheric electrons are sufficient (e.g. during daytimes). In fact, there were two explosions of the Shin-Moe volcano (Feb.1 20:25 UT, and Feb. 13 20:07 UT) with stronger airwaves than the February 11 02:36 UT eruption. However, we cannot find ionospheric disturbances for these explosions because of small background VTEC early in the morning.

At last, we discuss the origin of the period of the observed TEC variations. As seen in Figure 3, TEC changes by the five different volcanic explosions have similar periods of ~1.3 minutes. Such a uniformity suggests its origin in the atmospheric structure rather than characteristics of the volcanic eruptions. In Figure 6, we compare this period with the diagram of atmospheric attenuation of acoustic waves with various periods at different altitudes (Blanc, 1983).

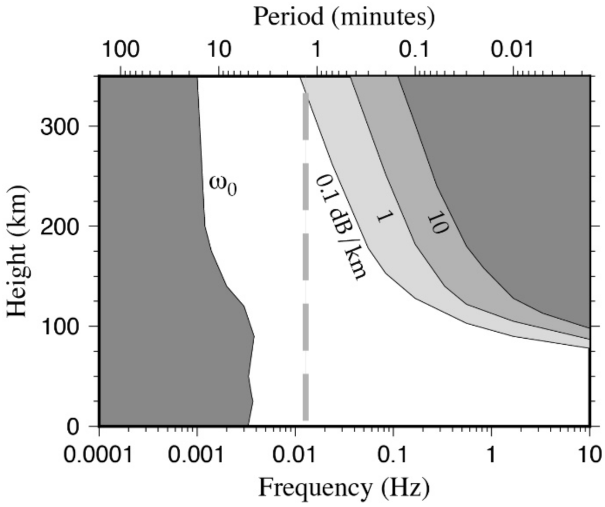

Figure 6. Frequency (~12.8 mHz) and period (~1.3 minutes) of TEC oscillations by explosive volcanic eruptions (vertical dashed line) drawn over the figure by Blanc (1983) showing the attenuation of airwaves in the Earth's atmosphere. The frequency 12.8 mHz corresponds to the higher end of the atmospheric bandpass filter.

Figure 6 shows that 1.3 minutes corresponds to the shortest period of the airwaves that can reach ionosphere without large attenuations, i.e. 12.8 mHz corresponds to the high end frequency of the atmospheric band-pass filter. Infrasound records observed at ground sensors associated with explosive volcanic eruptions have stronger powers in periods much shorter than 1.3 minutes (e.g. Matoza et al., 2019). However, only those with periods 1.3 – 4.0 minutes can reach the ionospheric F region. Because the original spectrum had larger powers for higher frequencies, we would have detected the 12.8 mHz component as the TEC changes at the F region altitude (~300 km).

Acknowledgements

We thank two reviewers for constructive reviews. This research was supported by the World Class Professor 2019 program by the Indonesian government.

References

Blanc, E. (1985), Observations in the upper atmosphere of infrasonic waves from natural or artificial sources: A summary, *Ann. Geophys., 3*(6), 673–688.

Cahyadi, M. N., R. W. Rahayu, K. Heki, and Y. Nakashima (2020), Harmonic Ionospheric Oscillation by the 2010 Eruption of the Merapi Volcano, Indonesia, and the Relevance of its Amplitude to the Mass Eruption Rate*, J. Volcanology & Geothermal Res.*, submitted.

Chonan, M. et al. (2018), Ionospheric disturbances associated with Mt. Asama eruption observed by GPS-TEC and HF Doppler sounding, paper presented at *the Japan Geoscience Union, General Assembly*, Chiba, May 20-24, 2018.

Dautermann, T., Calais, E., Mattioli, G. S. (2009a), Global Positioning System detection and energy estimation of the ionospheric wave caused by the 13 July 2003 explosion of the Soufrière Hills Volcano, Montserrat. *J. Geophys. Res., 114*, B02202, doi:10.1029/2008JB005722.

Dautermann, T., Calais, E., Lognonné P., Mattioli, G. S. (2009b), Lithosphere-atmosphere-ionosphere coupling after the 2003 explosive eruption of the Soufriere Hills Volcano, Monserrat. *Geophys. J. Int., 179*, 1537–1546, doi:10.1111/j.1365-246X.2009.04390.x.

Heki, K. (2006), Explosion energy of the 2004 eruption of the Asama Volcano, central Japan, inferred from ionospheric disturbances, *Geophys. Res. Lett., 33*, L14303, doi:10.1029/2006GL026249.

Hofmann-Wellenhof, B., H. Lichtenegger, and E. Wasle (2008) GNSS-Global Navigation Satellite Systems, Springer, doi:10.1007/978-3-211-73017-1.

Japan Meteorological Agency (Kagoshima Local Meteorological Observatory, and Fukuoka District Meteorological Observatory) (2010), Volcanic activity of Sakurajima volcano – October 2009 – January 2010 -, Report to Coodinating Committee for Prediction of Volcanic Eruption, Japan, *Report No.105*. (in Japanese)

Japan Meteorological Agency (Fukuoka District Meteorological Observatory and Kagoshima Local Meteorological Observatory) (2013), The 2011 Eruptive Activities of Shinmoedake Volcano, Kirishimayama, Kyushu, Japan, Quarterly J. Seism., 77, 65-96. (in Japanese with English abstract)

Japan Meteorological Agency (Fukuoka District Meteorological Observatory and Kagoshima Local Meteorological Observatory) (2015), Volcanic activity of the Kuchinoerabu-jima in 2015, https://www.data.jma.go.jp/svd/vois/data/tokyo/STOCK/monthly_v-act_doc/fukuoka/2015y/509_15y.pdf. (in Japanese)

Mannucci, A. J., B. D. Wilson, D. N. Yuan, C. H. Ho, U. J. Lindqwister, & T. F. Runge (1998), A global mapping technique for GPS-derived ionospheric total electron content measurements, *Radio Sci., 33*, 565–582, doi:10.1029/97RS02707.

Matoza, R., Fee, D., Green, D., Mialle, P. (2019), Volcano infrasound and the international monitoring system in *Infrasound Monitoring for Atmospheric Studies*, edited by Le Pichon, A., Blanc, E., and Hauchecorne, A., pp.1023-1077, Springer, Cham, ISBN:978-3-319-75138-2.

Nakada, S., M. Yoshimoto, E. Koyama, H. Tsuji, and T. Urabe (2005), Comparative study of the 2004 eruption with old eruptions at Asama Volcano and the activity evaluation, *Kazan, 50*, 303-313. (in Japanese with English abstract)

Nakashima, Y. (2018), Multi-sensor study of dynamics of atmospheric waves induced by volcanic eruptions. *PhD Thesis*, Hokkaido University.

Nakashima, Y., K. Heki, A. Takeo, M. N. Cahyadi, A. Aditiya, and K. Yoshizawa (2016), Atmospheric resonant oscillations by the 2014 eruption of the Kelud volcano, Indonesia, observed with the ionospheric total electron contents and seismic signals, *Earth Planet. Sci. Lett., 434*, 112–116, doi:10.1016/j.epsl.2015.11.029.

Occhipinti, G., Rolland, L., Lognonné, P., Watada, S. (2013), From Sumatra 2004 to Tohoku-oki 2011: The systematic GPS detection of the ionospheric signature induced by tsunamigenic earthquakes. *J. Geophys. Res. Space Phys., 118*, 3626O, doi:10.1002/jgra.50322.

Rolland, L. M., M. Vergnolle, J.-M. Nocquet, A. Sladen, J.-X. Dessa, F. Tavakoli, H. R. Nankali, and F. Cappa (2013), Discriminating the tectonic and non-tectonic contributions in the ionospheric signature of the 2011, Mw7.1, dip–slip Van earthquake, Eastern Turkey, *Geophys. Res. Lett., 40*, doi:10.1002/grl.50544.

Shults, K., Astafyeva, E., Adourian, S. (2016), Ionospheric detection and localization of volcano eruptions on the example of the April 2015 Calbuco events. *J. Geophys. Res. Space Physics, 121*, 10,303–10,315, doi:10.1002/2016JA023382.

Yokoo, A., F. Maeno, and H. Taniguchi (2005), Asama explosion of September 1st, 2004 – On the damage to glass windows and estimation of explosion energy, *Kazan, 50*, 195-201. (in Japanese with English abstract)